Final report: "Singlet Oxygen Generation Mediated by Silicon Nanocrystal Assemblies" W911NF-08-0011

Approved for Public Dissemination: Distribution Unlimited

Introduction

The purpose of this project was investigation and exploitation of the unique role of silicon nanocrystals as activators for photoexcitation of oxygen molecules. At first sight, one might expect the interaction between silicon and oxygen to be no more than a simple oxidation process (producing SiO_2). However, we have discovered that, at the nanoscale, the interaction becomes much more interesting and controllable. Silicon (Si) nanostructures have the extraordinary property of acting as facilitators for the photo-excitation of adsorbed oxygen molecules. Incident light creates excitons in Si nanostructures and these transfer energy to the adsorbed oxygen molecules.

We focused on the development of nanosilicon-based materials having required morphological and optical properties for the efficient generation of reactive singlet oxygen. Photosensitizing properties of silicon (Si) nanocrystal assemblies in different forms: porosified Si wafers and powders, freestanding spherical Si nanopowders etc have been studied. All relevant parameters of the system: singlet oxygen generation efficiency, stability of these systems under illumination, ageing effects and the influence of nanocrystal surface termination were investigated in detail. Chemical reactivity of singlet oxygen generated in gaseous and liquid phases has been studied using various organic molecules. Finally, prototypes of photochemical flow reactors utilizing porosified Si powders and microreactors based on porosified channels of etched Si wafers have been developed.

Scientific and technological objectives of the project

1. Development of technological processes for the formation of nanosilicon materials in different phases, with controllable sizes of particles in the range of 2-10 nanometers and in quantities sufficient for feasibility studies.
2. Comprehensive study of nanosilicon as a photo-sensitizer material for generation of singlet oxygen in the liquid and the gas phase. Definition of absolute yield of singlet oxygen under specified illumination conditions.
3. Control of long-term sensitization ability of Si nanocrystals assemblies.

Report Documentation Page

Form Approved
OMB No. 0704-0188

1. REPORT DATE	2. REPORT TYPE	3. DATES COVERED
2011		**00-00-2011 to 00-00-2011**

4. TITLE AND SUBTITLE	5a. CONTRACT NUMBER
Singlet Oxygen Generation Mediated By Silison Nanocrystal Assemblies	5b. GRANT NUMBER
	5c. PROGRAM ELEMENT NUMBER
6. AUTHOR(S)	5d. PROJECT NUMBER
	5e. TASK NUMBER
	5f. WORK UNIT NUMBER
7. PERFORMING ORGANIZATION NAME(S) AND ADDRESS(ES) **Department of Physics ,University of Bath,Bath BA2 7AY, UK, ,**	8. PERFORMING ORGANIZATION REPORT NUMBER
9. SPONSORING/MONITORING AGENCY NAME(S) AND ADDRESS(ES) **ERDC-IRO, Richmond, Unit 5760, APO AE 09421, , , ,**	10. SPONSOR/MONITOR'S ACRONYM(S)
	11. SPONSOR/MONITOR'S REPORT NUMBER(S)

12. DISTRIBUTION/AVAILABILITY STATEMENT
Approved for public release; distribution unlimited

13. SUPPLEMENTARY NOTES
: 1244-EN-01 / Contract no: W911NF-08-2-0011 / Prof. Dmitry Kovalev of the University of Bath / Singlet oxygen generation mediated by silicon nanocrystal assemblies.

14. ABSTRACT

15. SUBJECT TERMS

16. SECURITY CLASSIFICATION OF:			17. LIMITATION OF ABSTRACT	18. NUMBER OF PAGES	19a. NAME OF RESPONSIBLE PERSON
a. REPORT	b. ABSTRACT	c. THIS PAGE			
unclassified	**unclassified**	**unclassified**	**Public Release**	**33**	

4. Feasibility studies of chemical transformations of organic molecules.

5. Development of PSi-based photochemical reactors

Main outcomes of the project

In order to achieve the main objectives we realized:

1 Development of different methods of scalable synthesis of nanoporous silicon (PSi) and freestanding Si nanocrystals with different pore sizes and distributions between 2 and 10 nm. In addition to the synthesis, these new materials were characterized by volumetric adsorption technique, IR and Raman spectroscopies. These methods provided important information on morphology of nanosilicon materials and their surface chemistry. Stability of nanosilicon materials has been determined for oxygen and air ambient as well as for oxygen-saturated water.

2 Study of singlet oxygen generation mediated by PSi by steady state and time-resolved photoluminescence measurements. Rates of singlet oxygen generation and steady state concentration have been determined and these parameters have been used for kinetic modeling.

3 Study of energy/charge transfer mechanisms that result in desired chemical transformations of different organic molecules. Liquid reactions were performed in a flow photochemical reactor using different light sources.

4 Identification of basic mechanisms of molecular transformations and limiting processes. These studies enable further optimization of the photochemical processes.

5. Development of highly efficient microstructured Si-based photochemical flow reactors and microreactors based on Si wafers incorporating porous nanocrystalline silicon.

Our results have been published in several research articles devoted to new nanosilicon materials and singlet oxygen chemistry mediated by excitons confined in Si nanocrystals.

1. Fabrication of different nanosilicon in quantities sufficient for its practical application.

1.1 Electrochemically etched Si wafers

We developed deep electrochemical etching technique to anodize full 4´´ Boron-doped Si wafers up to the depth of 500 μm. This allows to produce ~ 0.5 gram of PSi per 4´´ bulk Si wafer. Sketch of the etching cell is shown in Fig. 1. Depending on wafer doping level and etching current values growth parameters were identified. PSi powders were produced via electropolishing step (current density is 500 mA/cm^2) followed by destructive sonification or ball milling of PSi layers. These procedures result in micrometer-sized PSi powders, which can be used in photochemical reactor.

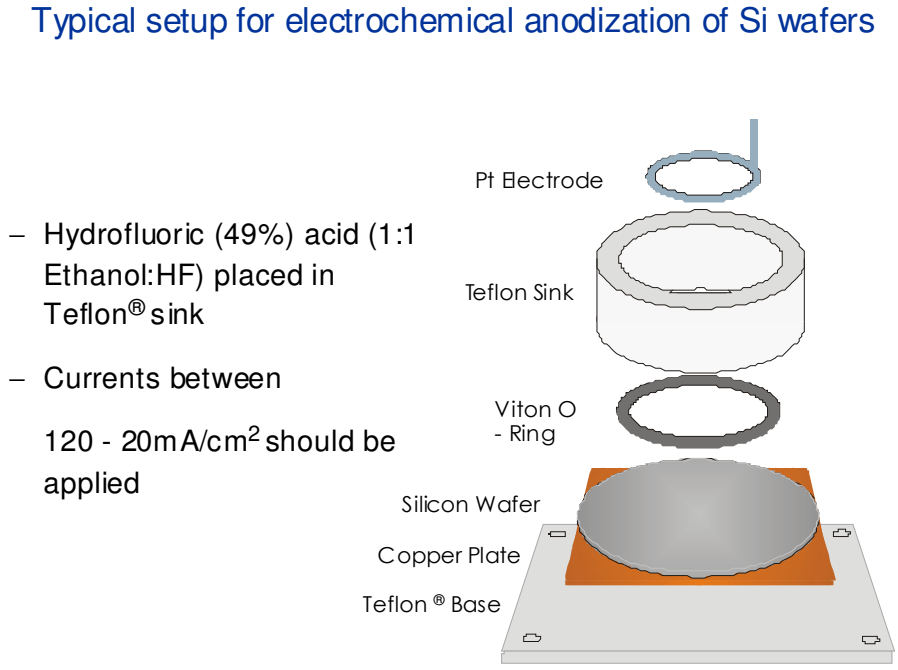

Fig. 1. Sketch of the electrochemical setup used for porosification of bulk Si wafers.

Electrochemical etching results in the formation of mechanically stable nanocrystaline Si network. Structural investigations have confirmed that PSi layers consist of Si nanocrystals having sizes dependent mainly on the doping level of wafers. Fig. 2 demonstrates typical TEM images of PSi layers etched using different Si substrates.

Due to quantum confinement effects and a distribution of sizes and shapes of the Si particles, the effective band gap energies of the nanocrystal assemblies range from

1.12 eV (p^{++} wafers) up to 2.1 eV (for p^- wafers and 100 mA/cm^2 current density). Since for the effective singlet oxygen generation excitons luminescing above 1.63 eV (excitation energy of singlet oxygen molecule) are required, only PSi produced from p^- Si wafers can be used. We estimated the output of nanosilicon powder from one 4´´ Si wafer to be up to 0.5 gram and the etching time required is 4 hours. Therefore while this etching technique is very useful for model experiments it clearly does not provide scalable root for the production of Si nanocrystals. Additional complication is a relatively large size of PSi grains. Both, sonification and ball milling techniques result in the PSi grains size in micrometer to ten´s of micrometers range.

Therefore we developed wet etching technique which results in scalable production of PSi.

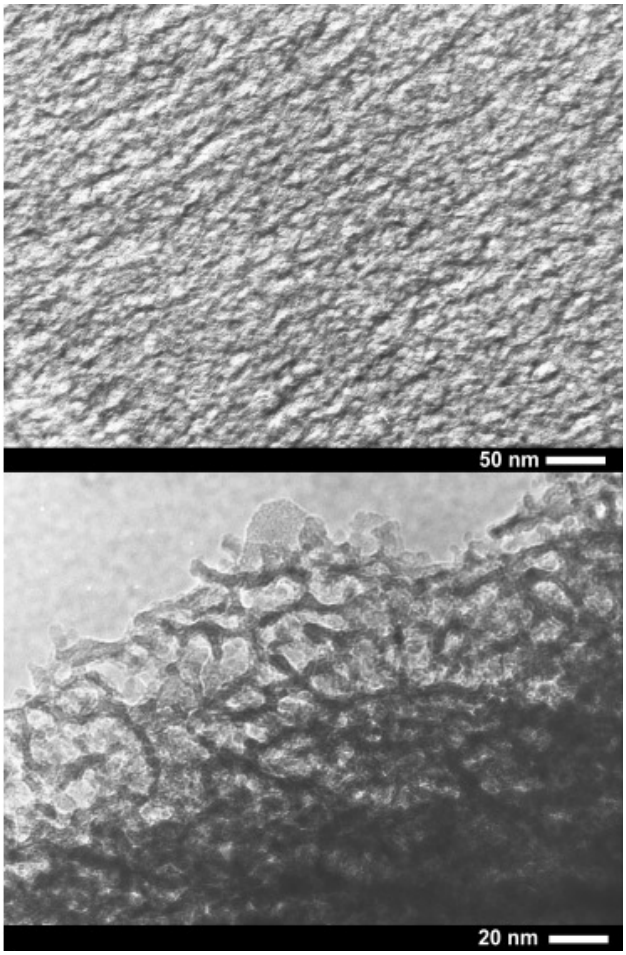

Fig 2. TEM images of electrochemically etched single-crystalline (100) p^+ (10 mΩ·cm) and p^- (1-5 Ω·cm) Si wafers in HF(49%):C_2H_5OH=1:1 solution. The etching current density is 50 mA/cm^2.

1.2. Strain etching of crystalline Si wafers and polycrystalline Si powders

Probably the most important decision which has to be me made is a proper choice of initial material before the etching. According to low costs requirement we selected stain-etched metallurgical quality micrometer-sized Silicon powder. For these studies we used standard metallurgical grade polycrystalline Si powders having mean grain size from ~2 to 20 μm commercially produced by Vesta Ceramics, LLC via milling procedure. Stain etching procedure has been used to achieve porosification of Si powders. According to our measurements using energy dispersive X-ray spectroscopy the elemental composition of the metallurgical Si powder is: Si: 95.97%, O: 3.67%, Al: 0.31%, As: 0.05%. The presence of B or Al provides the accumulation of holes at Si-etching solution interface which is essential for PSi formation. The wafers or powder were immersed in a 2:1:10 etching solution of $HF:HNO_3:H_2O$ and were etched for 2-4 min and 1-1.5 hours, respectively, to achieve different size distributions of Si nanocrystals.

We found that stain etching technique for Si wafers depth of PSi layers is limited by 2-4 μm and prolonged etching always result in slow dissolution of the porous Si layer. Therefore it has been decided that for further studies nanoporous Si will be produced mainly from polycrystalline Si powders.

For powders a permanent mixing was required since the H-terminated Si surface is hydrophobic and most of the powder was at the surface of the solution in the form of foam. The etching was finished when the initially metallic colour of the wafer or powder was changed to brown-yellow and simultaneously an efficient red-orange emission under illumination by ultraviolet light appeared. Increase of the etching time results in significant increase of the quantum yield and shift of the emission band towards higher energies. The porous powder was collected from the etching solution and dried at 100° C for 30 minutes or in vacuum for 10 hours. While after etching the residual mass of the nanostructured powder is about 10% of the initial bulk powder mass, measurements using scanning electron microscopy show that size distribution of nanostructured grains is almost the same as for bulk powder. Therefore, we concluded that the major part of this mass loss is due to porosification of Si grains. Fig.3 shows typical morphology of porosified Si powders. Nanosponge structure of porosified particles having sizes in the range of 3-7 nm is clearly seen. The lattice fringes in the HRTEM image correspond to (111) planes of Si nanocrystals, thus Si nanocrystals retain the diamond crystalline structure of bulk Si. The crystalline orientation of neighbouring Si nanostructures is according to the HRTEM images is the same because their sizes and mean distances

between them are far below the sizes of possible crystalline domains within polycrystalline grains.

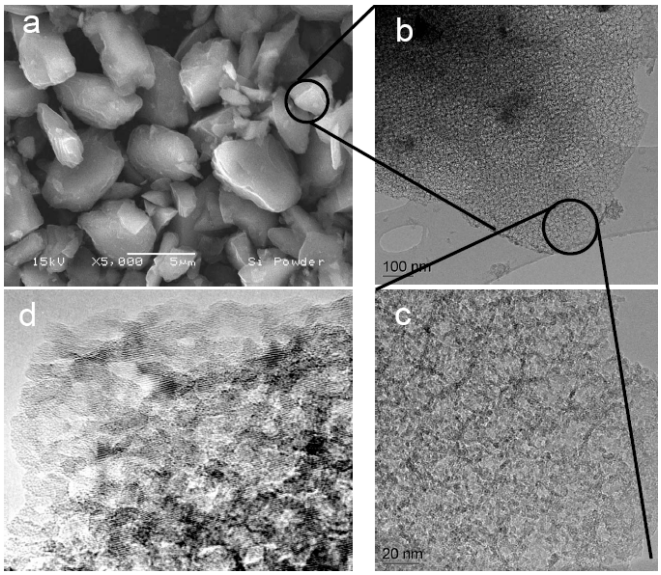

FIG. 3. SEM (a) and HRTEM (b-e) images of stain-etched Si powder. Lattice fringes in Fig.3 d correspond to the (111) atomic planes of Si nanocrystals. Length scales are indicated.

Downscaling of the stain etched PSi material crucially depends on the availability of the raw crystalline Si powder with a submicron mean size distribution. This material is not available on the industrial market since ordinary ball milling technique results in mean particle size of about 1 micrometer. Therefore it was necessary to develop new production method resulting in large quantities of free standing nanosized particles. Therefore as initial material we selected recently developed experimental product of Dr. Hartmut Wiggers (University of Duisburg, Germany). Silicon nanoparticles were produced in reactor via decomposition of silane either by infrared laser pulse or by microwave radiation. First techniques allows to produce crystalline Si particles with mean size ~ 200 nm and second one ~20 nm. Surface of particles after first preparation step is not passivated and their sizes are too large to achieve noticeable quantum size effects. Therefore second preparation step which will assure reduction of particles size and passivation of their surfaces was required. Again we selected stain etching technique to achieve these goals. Fig. 4a and 4b shows high resolution TEM image of nanostructured ~ 200 nm and ~ 50 nm large particles.

a) **b)**

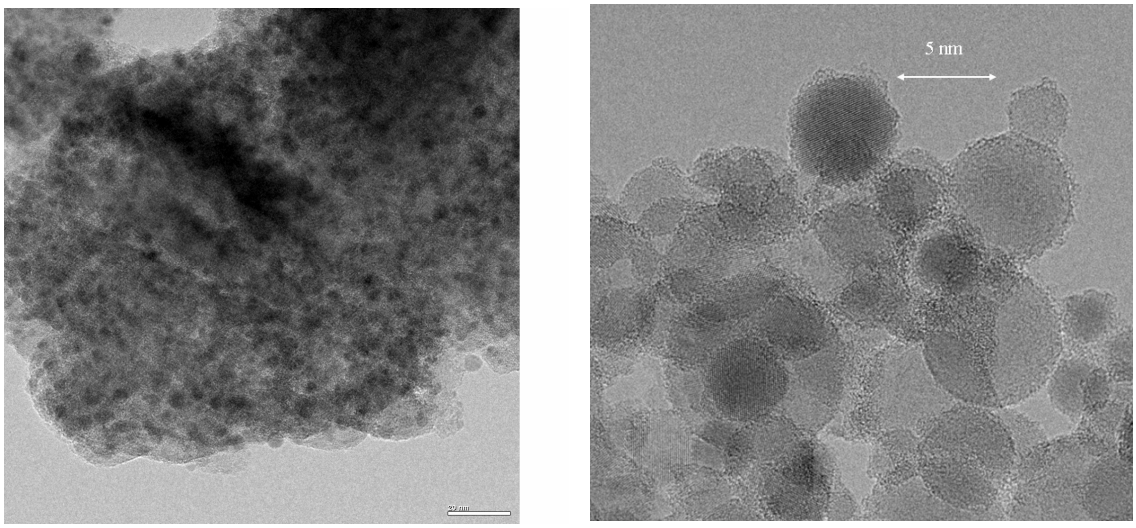

Fig. 4 a) HRTEM image of porosified single grain having size in the range of 200 nm. b) Luminescing Si nanospheres prepared using stain etching technique from initial nonluminescing Si spheres in the size range 20-50 nm. After nanostructuring typical size of Si nanocrystals is ~ 5 nm.

After stain etching procedure. 200 nm large porosified Si grains consist from almost ideal nanosilicon spheres with mean size ~ 5 nm (see Fig. 4 a). For this range of sizes quantum confinement effects becomes very important and efficient light emission can be detected. Fig. 4b demonstrates free standing nanosilicon spheres prepared by the procedure described above. These nanospheres have size in the range of 2-10 nm and also exhibit efficient light emission at room temperature. We found that dry stain-etching technique using vapors of the same acids is also a proper choice for achieving efficient photosensitizing activity of Si nanocrystals assembling particles. The largest size of particles which can be treated using this technique is found to be in the range of 4 μm.

Taking into account all structural, luminescing and photosensitizing properties of different nanosilicon-containing materials we decided that only stain-etched polycrystalline Si powders having grain sizes in the range 20 nm - 4 μm can be used for photochemical applications. Their production, contrary to other nanosilicon materials, is scalable and already up to 50 gram batch size was achieved in laboratory environment.

2. Surface termination of PSi: thermal oxidation and ageing in natural ambient environment. Photooxidation of PSi in water.

The surfaces of nanocrystals play a key role in virtually all of their properties, from light emission to solubility of nanocrystals in water. Freshly electrochemically formed nanosilicon is hydrogen passivated (see Fig. 5). While exposed to environment hydrogen is gradually substituted by more stable oxygen through the mechanism of back-bonding of oxygen atoms to the surface Si atoms. Under natural aging conditions main part of hydrogen still remains on the surface of Si nanocrystals. This effect *a-priory* should limit the duration of photosensitizing activity of nanosilicon to a few years.

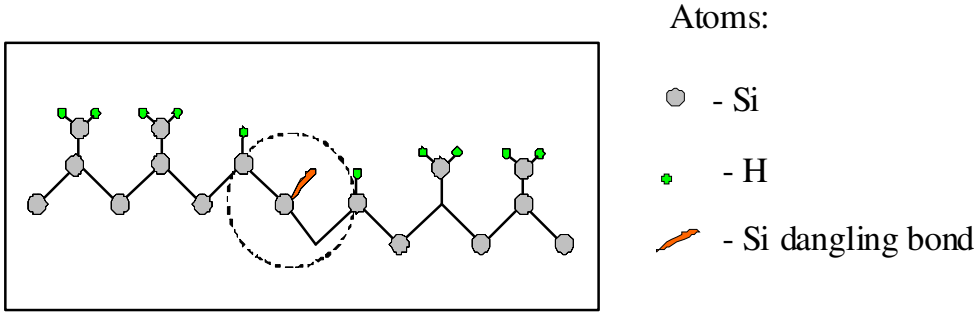

Fig. 5. Sketch of the surface of as-prepared PSi. Possible atomic configurations are shown. For Si nanocrystals dangling bonds play the role of nonradiative centres.

Surface composition of Si nanocrystals has been measured using infrared absorption spectroscopy. If powder is removed from the etching solution after complete consumption of HNO_3 in the etching solution nanocrystal surfaces are hydrogen-terminated and the amount of surface Si-O bonds is negligible (see Fig. 6). Otherwise, a significant amount of Si-O bonds dependent on the amount of remnant HNO_3 is detected. Therefore in all following studies complete consumption of HNO_3 during stain etching procedure has been achieved.

Natural ageing of powder in normal ambient during one year results in one monolayer of oxygen atoms back-bonded to the surface of Si nanocrystals and afterwards surface is completely stabilized. Integral absorption of (Si-)Si-H and (O-)Si-H bonds remains constant during ageing process and, therefore, total number of surface hydrogen atoms is preserved in the system. The same affect can be achieved due to artificial ageing of Si nanocrystals assemblies at elevated temperatures in natural ambient. We performed

a comprehensive study of the impact of thermal treatment of PSi on the surface termination of PSi.

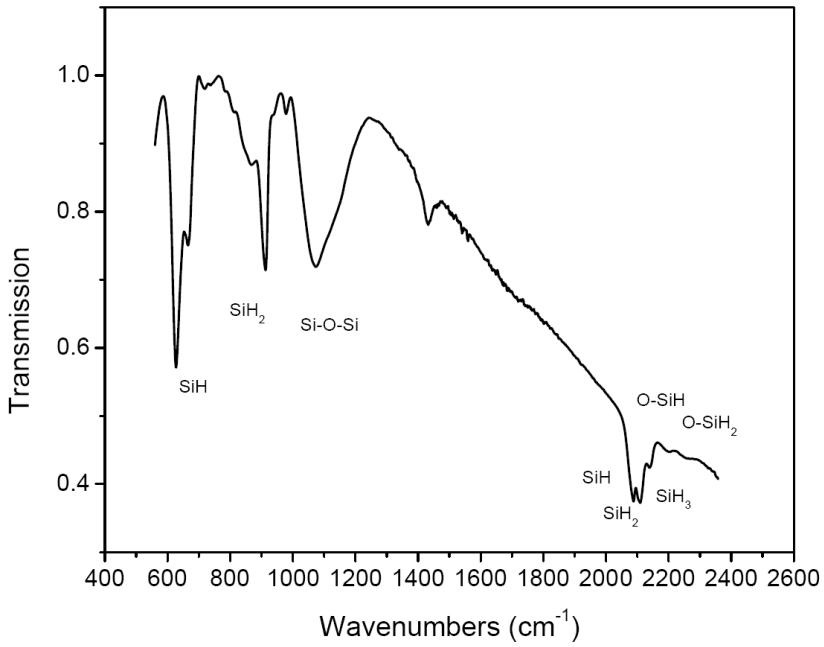

Fig. 6. Infrared absorption spectrum of as-prepared nanosilicon powder. Surface bonds are indicated. Si-O bonds can be seen even for very small concentration due to much larger oscillator strength than that of Si-H bonds.

Fig. 7 shows infrared absorption spectra of as-prepared PSi and PSi after thermal annealing in air ambient. While initially PSi has H-terminated surface, annealing in air at temperatures between 120 ^{o}C and 270 ^{o}C results in formation of one monolayer of back-bonded oxygen (similar to oxidation process at room temperature after 1 year). At temperatures above 300 ^{o}C hydrogen atoms are removed from the surface due to effusion process and a monolayer of Si-O is formed at the surface. Heating in vacuum does not affect surface composition of Si nanocrystals up to ~ 270 ^{o}C, afterwards a gradual effusion of hydrogen from the surface of Si nanocrystals can be detected.

Thus heating of nanosilicon structures which results in a removal of chemical residuals remaining after stain etching in the pores of PSi has to be performed in vacuum.

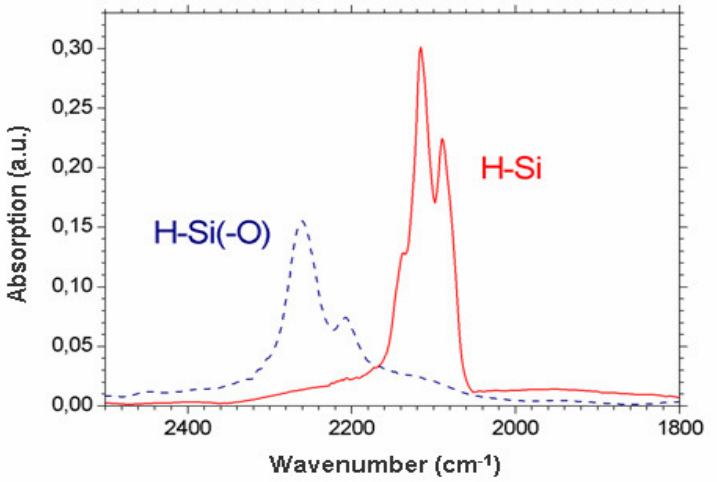

Fig. 7. Surface termination of as-prepared PSi (red curve) and of PSi after heating in air ambient at 200 ºC for 30 minutes. Formation of monolayer of back-bonded oxygen can be readily seen (blue curve).

Below we list most important specific observations relevant to PSi thermal annealing procedure performed in high vacuum.

1. Heating to 150 ºC in vacuum (10^{-5} mbar) does not influence significantly photoluminescence quantum yield of all tested Si nanostructures and singlet oxygen generation rate (20% reduction has been noticed for Si nanoparticles having size 3-5 nm).
2. Heating above 200 ºC gradually decreases both quantum yield of photoluminescence and singlet oxygen generation rate.

3. Heating above 300 ºC results in effusion of hydrogen atoms from the surface of Si nanocrystals and under these conditions neither photoluminescence nor singlet oxygen generation can be detected.

4. During heating presence of a water vapor should be avoided because it induces fast oxidation of silicon nanocrystals surfaces what increases PL quantum yield but significantly decreases singlet oxygen generation rate. Partially oxidized surfaces of Si nanostructures are generally more stable under the same conditions but singlet oxygen generation rate is relatively low.

5. Sub-micron suspensions (even nanometer-sized) can be heated up to 150 ºC but compromise between their stability and efficiency of singlet oxygen generation should still be found (identical to other photosensitizers).

Surface termination of PSi immersed in water naturally containing dissolved oxygen depends strongly on the illumination conditions. Photogenerated excitons can efficiently transfer energy to oxygen molecules and excite them in highly chemically reactive singlet oxygen. The result of the singlet oxygen attack on the surface of Si nanocrystals is very similar to thermal oxidation process in the temperature range between 120 ^{o}C and 270 ^{o}C. It also results in the formation of oxygen back-bonded to surface Si atoms (see Fig. 8). At illumination intensity of 1W/cm^2 in a time scale of a few hours a monolayer of oxygen is formed on the surface of Si nanocrystals.

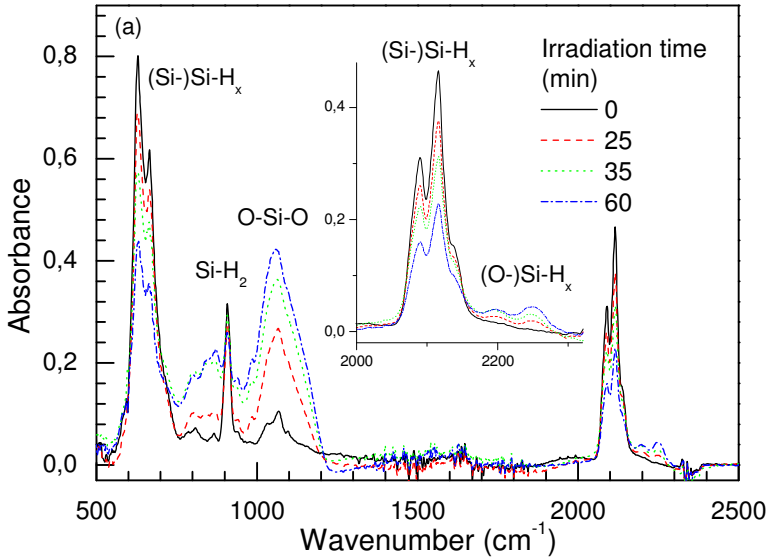

Fig. 8. Infrared absorption spectra of nanosilicon powder: as-prepared (solid line) and immersed in oxygen-containing water after illumination (doted lines). Irradiation time and surface bonds are indicated. Inset Infrared absorption spectra in the optical range of Si-H bonds.

All oxidation processes reduce singlet oxygen generation rate. However oxidized PSi can be refreshed via its immersion to HF-containing solution or via exposure to HF vapor. This procedure efficiently removes surface oxide. Hydrogen passivation of the surface of PSi is crucial for its application as an efficient singlet oxygen generator.

3. Study of PSi as a photo-sensitizing material for efficient generation of singlet oxygen in gas and liquid phase

3.1 Study of the efficiency of singlet oxygen generation as a function of nanocrystal size distribution, morphology and quantum yield of photoluminescence

The PL from PSi layers and PSi powders, depending on mean sizes of Si nanocrystals, can be continuously tuned with small increments over a very wide spectral range from the bulk Si band-gap to the green range for the smallest nanocrystals. Thus, the confinement energy can be more than 1 eV, as large as the fundamental bulk silicon band gap itself. This observation is crucial for the effect of photosensitization of molecular oxygen: the energy of excitons can be adjusted to any desirable value from 1 eV to 2.2 eV simply by a proper choice of Si nanocrystals sizes. Excitons having energies in the vicinity of $^3\Sigma$ - $^1\Sigma$ transition (1.63 eV) most efficiently excite O_2 to a singlet state. Therefore Si nanocrystals assemblies having PL band maximum at 1.63 eV are the best candidates for the efficient singlet oxygen generation. This can be seen

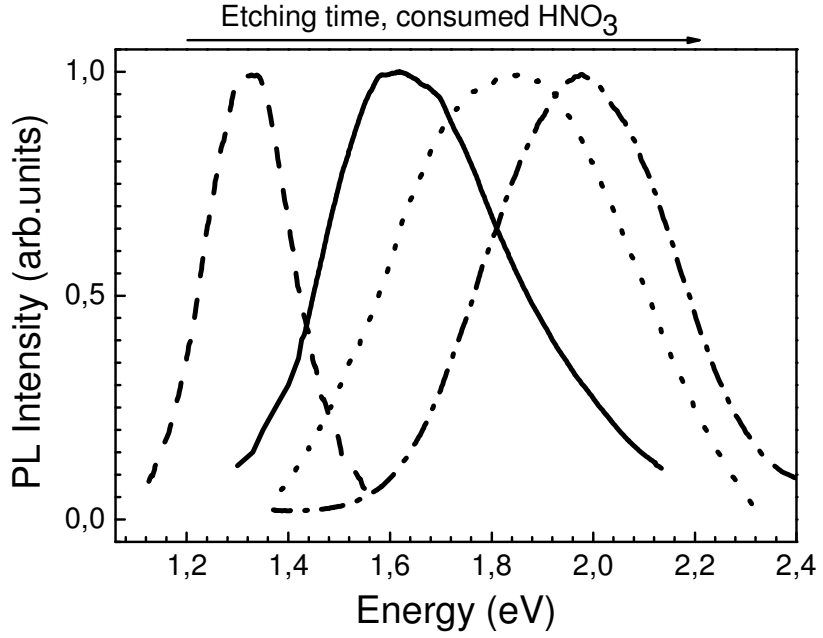

Fig. 9. PL spectra of differently prepared porosified Si powder.

Prolonged stain etching of Si polycrystalline grains results in their deeper porosification, reduction of nanocrystal size and better passivation of surface nonradiative centers – “dangling” Si bonds at the surface of Si nanocrystals.

as a blue shift of the PL band and as continuous increase of PL quantum yield and, therefore, singlet oxygen generation rate. Fig. 10 shows how PL intensity and singlet oxygen generation rate is developed during stain etching process. Since all bulk Si material can be completely dissolved during stain etching process we concluded that photosensitizing applications the optimal material is produced when is about 5% of initial mass of Si powder remains in the etching solution.

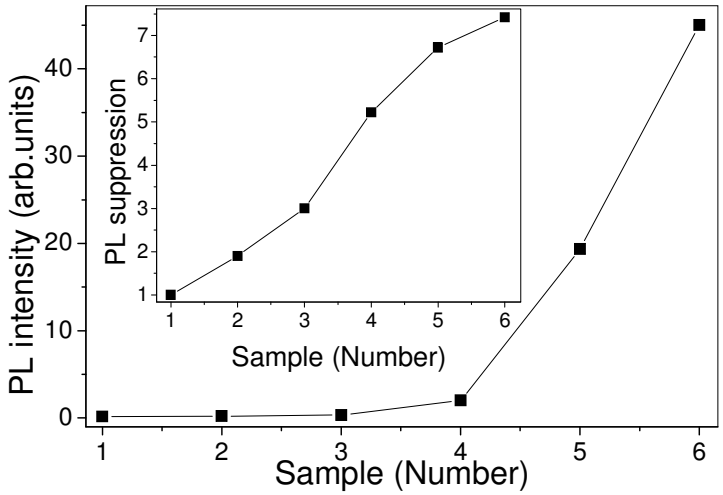

Fig. 10. PL intensity as a function of continuously prolonged etching of Si powder. Inset: PL suppression level (can be scaled as singlet oxygen generation rate) for the same samples.

The generation rate of singlet oxygen scales also with quantum yield of photosensitizer PL and its PL lifetime. In general, electrochemically etched Si wafers exhibit much smaller quantum yield of the PL than stain-etched Si powder.

Excitation of oxygen molecules to excited singlet states proceeds via energy transfer from photoexcited excitons confined in Si nanocrystals to oxygen molecules. Physically it can be seen as a difference of PL intensities in vacuum and in oxygen ambient (PL suppression level). We found that this quantity, which in fact defines the efficiency of singlet oxygen generation, depends strongly on the morphology of Si nanocrystal assemblies and their surface termination. Fig. 11 shows PL suppression levels for 3 types of nanosilicon used in our experiments. For PSi grains the PL suppression level is

around 9. This implies that the efficiency of singlet oxygen generation (the ratio of the number of singlet oxygen molecules to the number of photoexcited Si nanocrystals) is about 90%.

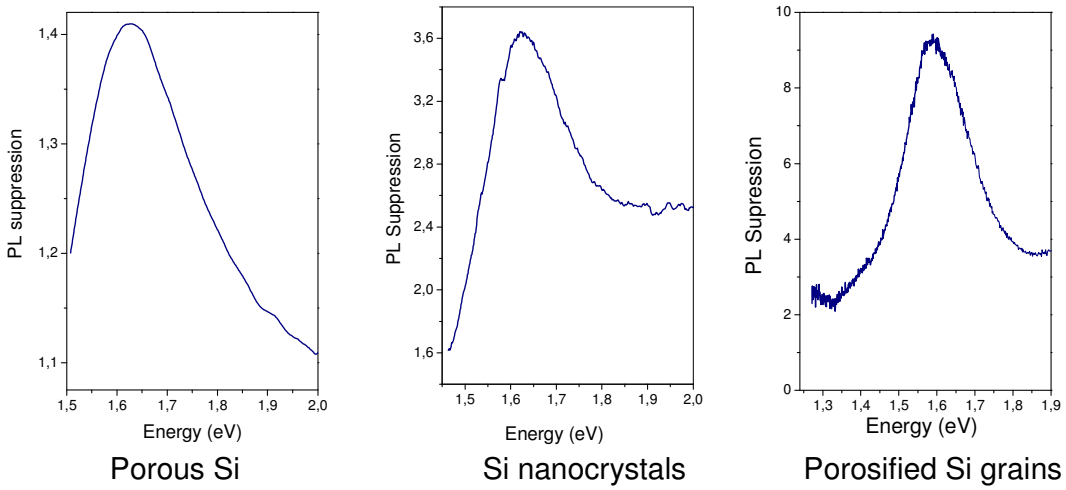

Fig. 11. PL suppression level in oxygen ambient at P=1 bar for electrochemically etched PSi, freestanding Si nanocrystals and PSi grains prepared via stain etching procedure.

This allows us to estimate the generation rate of singlet O_2 at room temperature in the pores of PSi.

For ambient O_2 pressure and 1 W/cm^2 excitation intensity at $E_{ex.}$=2.54 eV it gives ~ 5·10^{20} singlet oxygen molecules/cm^3·s.

The surface of nanocrystals plays a key role in their light emission properties and photosensitizing activity. Specifically for Si nanocrystals, three completely different types of surfaces can be realized. As-prepared PSi has a H-terminated surface. Thermal annealing of PSi in air at temperatures below 300 ^{o}C or its long-term ageing in air ambient results in the incorporation of a monolayer of oxygen atoms back-bonded to the surface of nanocrystals while hydrogen atoms still remain at the surface (hydrogen passivation of the surface is preserved). For Si nanocrystals having a monolayer of back-bonded oxygen the increased spacing between confined excitons and adsorbed oxygen molecules is on the order of 3 Å (double the length of the Si-O bond). A monolayer of incorporated oxygen also implies an additional potential barrier for the mutual tunneling of electrons.

This critically affects the efficiency of the electron exchange interaction and photosensitizing efficiency of Si nanocrystals. Contrary to a strong coupling for hydrogen-terminated nanocrystals, the PL quenching efficiency (and electron exchange

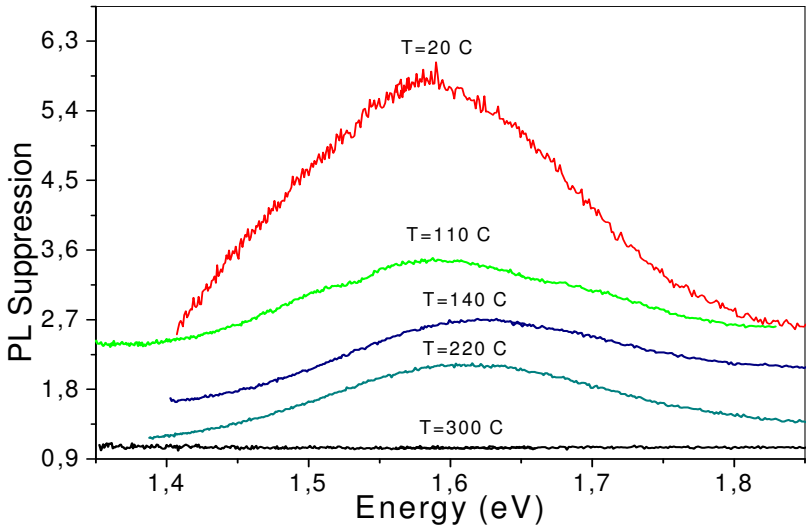

rate) is significantly reduced if a thin oxide barrier is present. We would like to note that

Fig. 12. PL suppression level (scaled as photosensitizing efficiency of Si nanocrystals) as a function of annealing temperature in the air (annealing time is 30 minutes). Annealing temperatures are indicated.

because the transition from H-terminated to O-terminated surfaces can be done smoothly via successive nanocrystals surface oxidation, the photosensitizing efficiency of Si nanocrystals assemblies, contrary to other systems, can be accurately controlled. At the same time singlet oxygen generation rate can be recovered via immersion of oxidized PSi in HF-containing solution or vapor which remove the surface oxide.

Thus to achieve the highest efficiency of singlet oxygen generation H-terminated as-prepared Si nanocrystals have to be used. Up to date stain-etched Si powder seems to be the best candidate for photosensitizing applications due to their higher stability against ageing.

3.2. Singlet oxygen generation in gas phase

The direct evidence of the photosensitized formation of singlet oxygen is obtained from PL excitation spectra. In Fig. 13 the intensity of the singlet oxygen PL (and, therefore, efficiency of singlet oxygen generation) is plotted as a function of the optical excitation

energy. We can see that singlet oxygen can be generated by light in a broad range of energies. However to achieve highest generation, short wavelength photons are required. The broad excitation spectrum is thus the direct evidence of the indirect excitation of singlet oxygen by the energy transfer from Si nanocrystals. This broad excitation spectrum demonstrates that any visible light sources (daylight, lamps, light emitting diodes, lasers) can be used to initiate singlet oxygen generation.

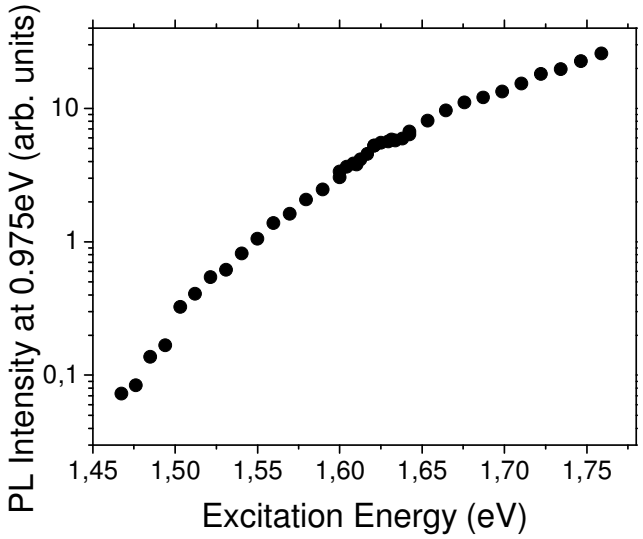

Fig. 13. PL intensity of singlet oxygen $^1\Delta$–$^3\Sigma$ emission line as a function of the excitation energy.

The very broad excitation spectrum covering a part of near IR and whole visible optical range provides significant advantage of systems containing Si nanocrystals for photosensitizing applications with respect to conventional sources. Absorption maxima of dye photosensitizers used for singlet oxygen generation are between 630 to 700 nm. On the other hand, Si nanocrystals can mediate generation of singlet oxygen under illumination by light having longer wavelength. This may significantly extend the applicability of Si nanocrystals as photosensitizers of O_2 for various purposes.

We studied kinetics of singlet oxygen generation with the aim to define time of the energy transfer from excitons confined in Si nanocrystals to molecular oxygen. These measurements (Fig. 14) show, that the energy transfer to MO is in the same time scale as the radiative exciton decay. For low energies this energy transfer is nearly three times faster than the radiative relaxation. To estimate the energy transfer time PL

kinetics have been measured in vacuum and in the ambient of molecular oxygen. Exciton lifetime in MO ambient is always shorter than in vacuum. The energy transfer time τ_{tr} can be found according to the simple relation $\tau_{meas} = \frac{\tau_{rad}.\tau_{tr}.}{\tau_{rad} + \tau_{tr}}$ where τ_{meas} and τ_{rad} are the measured PL lifetime in the presence of MO and the radiative exciton

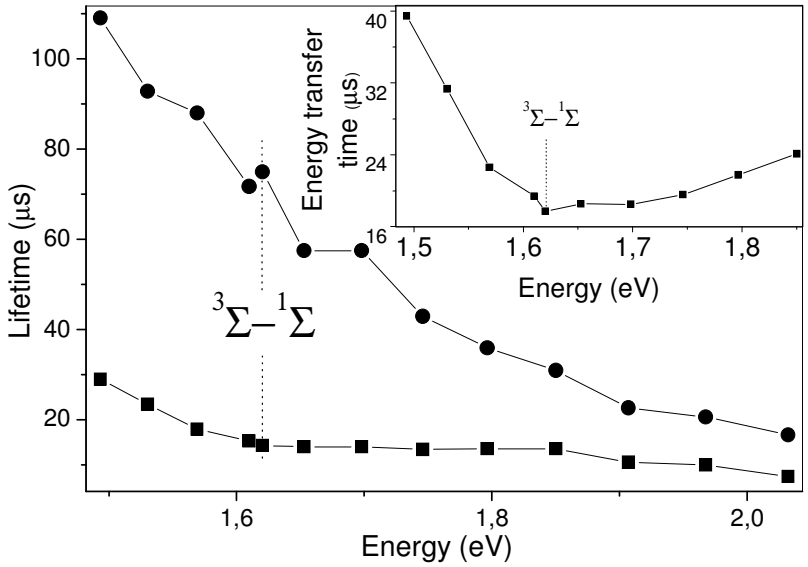

Fig. 14. Spectral dispersion of excitons lifetime in vacuum (circles) and at 1 bar of oxygen ambient (squares). Inset: spectral dispersion of the energy transfer time. Molecular oxygen transition energy is indicated.

lifetime in vacuum, respectively. The shortest τ_{tr} is about 18 μs at 1 bar of oxygen ambient when the energy of exciton coincides with the energy of the triplet–singlet transitions of oxygen molecule. This time becomes longer for higher and lower energies (inset of Fig. 14) but it is still faster than radiative exciton lifetime for almost all exciton energies. Therefore, the high efficiency of the singlet oxygen generation in gas phase at room temperature is a consequence of very long radiative lifetimes of excitons confined in Si nanocrystals.

Porosified H-terminated Si powder having grain size in the range of 1 - 4 μm demonstrates highest yield of singlet oxygen in gas phase and highest stability against natural oxidation. Its PL maximum can be easily adjusted to the desired 1.63 eV position. Additionally it can be easily produced in large quantities using simple laboratory equipment.

3.3. Generation of singlet oxygen in organic liquids and in water.

For many applications in chemical and biological fields, formation of singlet oxygen in solution is required; because singlet oxygen mediated reactions proceed usually in solution. Therefore the formation of singlet oxygen at room temperature must be proved without doubt only by detecting the near infrared emission from singlet oxygen. In most solvents, deactivation of singlet oxygen is radiationless by collisional electronic to vibrational energy transfer. The most probable energy-accepting oscillator of a solvent molecule is its terminal atom pairs with the highest vibrational energy (e.g., O-H, C-H). Therefore, to obtain reliable luminescence data, solvents consisting of poor quenchers have been chosen. Fig. 15 demonstrates spectroscopic evidence of singlet oxygen generation in hexafluorobenzene (C_6F_6).

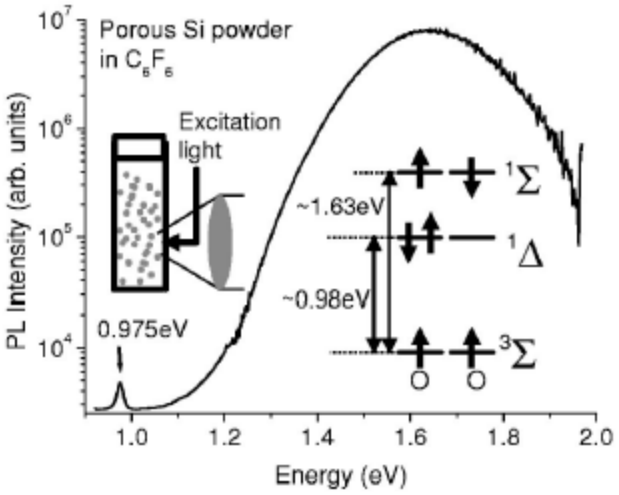

Fig. 15. PL spectrum of porous Si dispersed in C_6F_6 solution at room temperature. The peak at around 0.975 eV corresponds to the emission from singlet oxygen. Note logarithmic scale is used for the vertical axis.

It is interesting to note that at high level of optical excitation PL emission at 0.975 eV saturates, which implies that all oxygen molecules dissolved in C_6F_6 can be transferred to excited singlet state.

One of the purposes of the following work was to demonstrate the photosensitized generation of singlet oxygen in aqueous solution when Si nanocrystals are used as a photosensitizer. We demonstrated that the singlet oxygen PL line can clearly be detected when PSi is photoexcited in O_2 -saturated deuterated water (D_2O). We selected D_2O because its chemical reactivity is almost identical to H_2O but lifetime of

singlet oxygen in this solution is rather long what gives opportunity to observe generation of singlet oxygen via direct spectroscopic study. Fig. 16 a) shows how singlet oxygen generation rate depends on the amount of PSi powder immersed in D_2O.

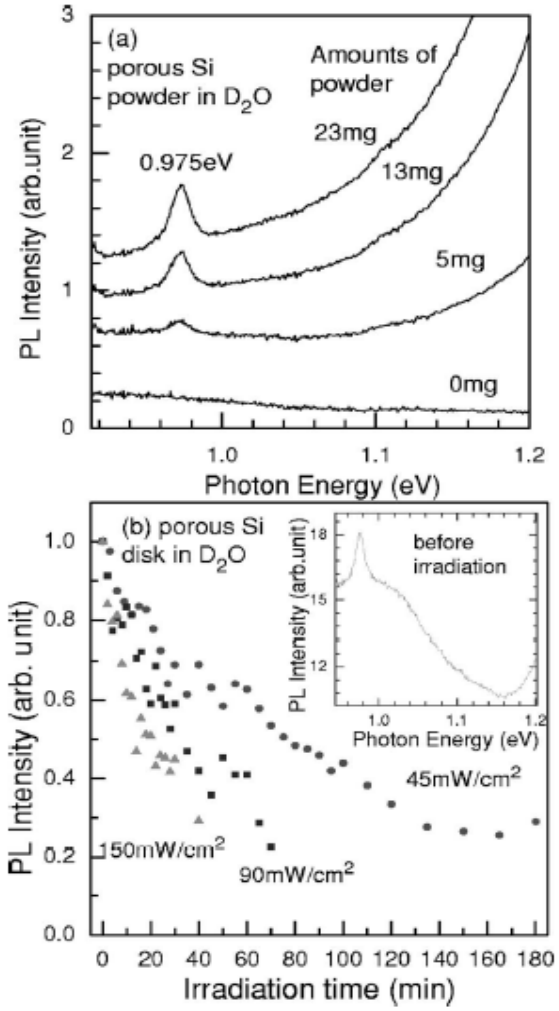

Fig. 16. a) PL spectra of D_2O solution containing various amounts of PSi powder. (b) PL intensity of singlet oxygen line detected at 0.975 eV as a function of irradiation time. The data are obtained for PSi disks in D_2O. A typical PL spectrum is shown in the inset.

Already at concentrations of PSi as low as 1 mg/cm^3 generation of singlet oxygen can be clearly seen. Probably on of the most crucial effect relevant to generation of singlet oxygen in aqueous solutions is its photodegradation due to photooxidation. This process drastically reduces photosensitizing ability of Si nanocrystals in a time scale of hours. Illumination of PSi in oxygen-saturated water results in its surface oxidation (see Fig. 8), formation of surface dangling bonds and, therefore, decrease of the intensity of

the PL and single oxygen generation rate. As can be seen in Fig. 16 b this process depends on the illumination level and proceed in a time scale of hours. As it was mentioned before oxide layer can be removed via sample “refreshment procedure”.

For chemical applications of singlet oxygen, its generation in oxygen-containing aqueous solutions is crucial. Unfortunately, fast nonradiative vibrational relaxation processes of singlet oxygen in H_2O makes the detection of singlet oxygen dissolved in water extremely difficult. However, even if the emission line is not detected, the energy transfer can be indirectly probed by monitoring the shape of the PL band and the lifetimes of excitons in the presence of dissolved O_2.

To obtain the spectral dependence of the energy transfer efficiency for oxygen-saturated water we use the procedure identical to that employed for gaseous O_2 ambient (see Fig. 14). Although the PL suppression level is weaker, its spectral shape is almost identical to that measured in gaseous O_2. This evidences the formation of singlet oxygen in water and evidences that the energy exchange mechanism should be identical. From the PL suppression level it follows that the efficiency of the energy transfer in oxygen-saturated water is equal to 75%.

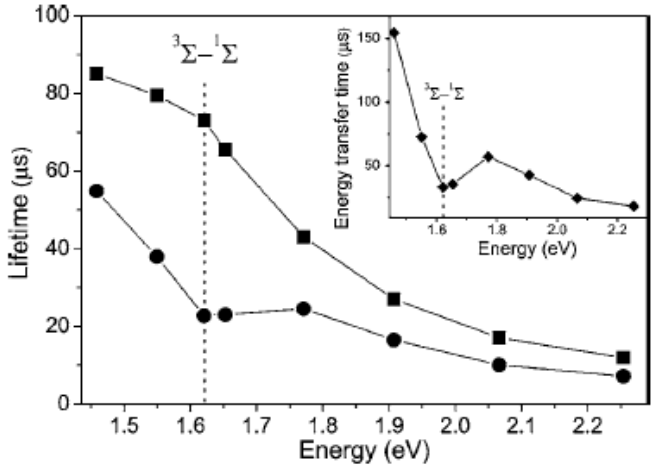

Fig. 17. Spectral dependencies of the PL lifetime measured in degassed water (squares) and in oxygen-saturated water (circles). Inset: spectral dependence of the energy transfer time in oxygen saturated water. T=300 K, $E_{ex.}$ =2.33 eV. Energy of the triplet-singlet oxygen transition is indicated by doted line.

Finally we determined the energy transfer time for oxygen-saturated water following the same procedure as for gaseous oxygen ambient (see Fig. 17). The exciton lifetimes for silicon nanocrystals immersed in degassed water are identical to those measured in vacuum. Oxygen dissolved in water causes its significant shortening over all spectral

range investigated. The spectral dependence of the energy transfer time is very similar to that observed for gaseous oxygen ambient (see inset of Fig. 17). A slightly longer energy transfer time of 30 microseconds is still shorter than the exciton lifetime what is in good agreement with the observed small difference in the PL suppression levels.
The observation that all oxygen molecules in D_2O can be efficiently transferred in the singlet state and taking into account the difference of singlet oxygen lifetime in H_2O and D_2O and solubility of O_2 in water allows us to estimate maximal values of two fundamental parameters of the system containing Si nanocrystals dissolved in water.

Singlet oxygen generation rate: for ambient conditions and 1 W/cm^2 excitation intensity it gives ~ 4·10^{20} singlet oxygen molecules/cm^3·s for air-saturated water.

Stationary concentration of singlet oxygen in air-saturated water : ~ 10^{15} singlet oxygen molecules/cm^3.

4. Study of mechanisms of interaction between porous silicon, oxygen and reactants

For many chemical applications, formation of singlet oxygen in solution is required; because singlet oxygen mediated reactions proceed usually in solution. The standard method to detect singlet oxygen in solution is to use chemical/biochemical traps (singlet oxygen acceptors) and analyze a specific reaction product or monitor the decrease in the amount of acceptor materials. We selected 1,3-diphenylisobenzofuran (DPBF) to monitor singlet oxygen formation via observation of the decrease in the intensity of the absorption band of DPBF. We study the absorption spectra of DPBF-dissolved solution containing porous Si powder under light irradiation and demonstrated that porous Si acts as a photosensitizer for singlet oxygen generation in solution.
For consideration of the mechanisms of interaction between oxygen, porous silicon and organic reactant molecules we used several test reactions and data of photoluminescence spectroscopy as well as NMR concentration measurements.
In general, the rate of photooxidation depends on the bimolecular rate constant and on the singlet oxygen steady-state concentration in solution. In equilibrium the rate of singlet oxygen generation, ϕI_a equals the rate of its decay $k_D[^1O_2]_{SS}$ and therefore steady state concentration of singlet oxygen is:

$$[^1O_2]_{SS} = \phi I_a / k_D \quad (1)$$

Here ϕ is quantum yield of singlet oxygen generation, I_a is the intensity of the absorbed light and k_D is the first order singlet oxygen decay constant. In the presence of singlet oxygen quencher R, steady state concentration of singlet oxygen is reduced:

$$[^1O_2]_{SS} = \phi I_a /(k_D + k_R[R]) \quad (2)$$

Here k_R is an overall rate constant for physical quenching and chemical reaction with singlet oxygen. Reduction in the steady state concentration of singlet oxygen in a solution can be detected as the decrease of singlet oxygen PL emission intensity at 1270 nm (0.98 eV). Therefore, using sensitive PL spectroscopy it is possible to monitor the photooxidation of different reactants and compare efficiencies of different sensitizers.

A decrease in singlet oxygen PL (or, respectively, of singlet oxygen steady state concentration) can take place either due to physical quenching or chemical reaction. In the case of the physical quenching, addition of a specific amount of quencher will result in the corresponding constant level of PL suppression. On the contrary, if chemical reaction path dominates, concentration of the reagent decreases with time, and consequently the level of singlet oxygen PL quenching should be reduced. The corresponding experiment has been done and its results are demonstrated in Fig. 18. In this case we used the reaction shown in the scheme below. This reaction is highly sensitive to the nature of the oxidizing species and can be used to detect the difference between singlet oxygen or superoxide.

Following the initial quenching of singlet oxygen PL with 75 μM of α-terpinene, the PL intensity recovered almost completely over 40 min of illumination by an Ar^+ laser (500 mW· cm^{-2} illumination intensity). This indicates a chemical reaction between singlet oxygen and α-terpinene. In Fig. 18 the PL signal without α-terpinene corresponds to the curve having the largest intensity, whereas the curve with the lowest intensity is recorded immediately after the addition of the reactant. The lines between these two limits from bottom to the top clearly show recovery of singlet oxygen luminescence after continuous illumination for 12, 21 and 40 minutes, respectively. This is easily seen in the inset in Fig. 18, showing the intensity of the singlet oxygen PL as a function of time. The overall singlet oxygen generation rate mediated by PSi is a product of the absorbed light intensity, the quantum yield of photogenerated long living excitons and the efficiency of energy transfer from photoexcited Si nanocrystals to oxygen molecules.

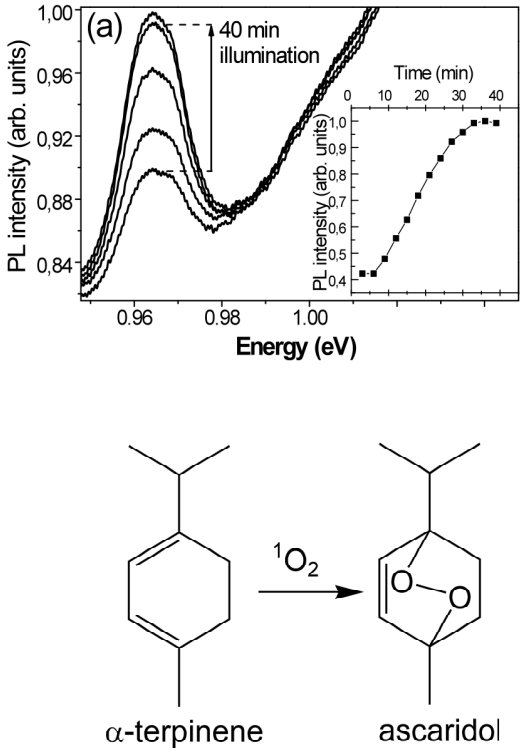

Fig. 18. Time evolution of the singlet oxygen PL spectra ($^1\Delta - {}^3\Sigma$ decay transition) after initial addition of 75 μM α-terpinene to 0.9 % wt. of PSi powder in C_6F_6, $I_{ex.}$= 500 mW·cm^{-2}, $E_{ex.}$= 2.54 eV. Insets: singlet oxygen PL peak intensity as a function of time for the respective images. The broad PL from Si defects was subtracted in order to estimate the PL intensity. Below is the graphical representation of the chemical reaction.

Despite the high efficiency of the latter process, which is about 80 %, the singlet oxygen generation efficiency cannot exceed 0.05-0.1, because quantum yield of PSi PL (or the number of long living excitons created by light per number of absorbed photons) does not exceed this value. Therefore, in the case of the PSi sensitizer the illumination time or intensity of light should be significantly increased to achieve similar conversions comparable with organic photosensitizers having quantum yield of singlet oxygen generation in the range of about 0.7-0.9.

Steady state concentration of singlet oxygen in the absence of added quenchers can be expressed by Eqn. (1). In the case of molecular organic photosenitizers, the singlet oxygen decays mostly due to collisions with molecules of solvent, and therefore, decay constant k_D is determined only by lifetime of singlet oxygen in a

particular solvent, τ_d. In the case of PSi an additional term, given by the deactivation time of singlet oxygen by the surface of Si nanocrystals, τ_q, contributes to the solvent-mediated quenching of singlet oxygen. It should be noted that the surface of Si nanocrystals is H-terminated and, due to high frequency of Si-H bonds oscillations, this surface can very efficiently quench singlet oxygen molecules during collisions. The total lifetime of singlet oxygen, τ_D, measured in suspensions of PSi (1 % wt) in C_6F_6 in the absence of other quenchers was found to be 3.9 ms. Taking into account this value and the lifetime of singlet oxygen in pure C_6F_6 (τ_d =25 ms) it is possible to estimate the deactivation time of singlet oxygen by the surface of Si nanocrystals, using Eqn. (3):

$$1/\tau_D = 1/\tau_d + 1/\tau_q \quad (3)$$

Based on this equation τ_q was estimated to be about 4.9 ms. This value implies that 84 % of photogenerated singlet oxygen is deactivated in PSi due to collisions with its hydrogenated internal surface.

Apart from quenching of excitons confined in Si nanocrystals by oxygen molecules, another possible deactivation pathway is direct quenching of excitons by organic molecules. Investigating the quenching of PL from PSi (suspensions of 1.1 % wt in DCM) using gradual addition of α-terpinene, or earlier studied DPBF, it was found that DPBF significantly suppresses PSi PL even in micromolar concentrations, see Fig. 19. About 0.7 mM was sufficient to quench all photoexcited excitons. Since the triplet state energy of DPBF lies about 1.48 eV above the ground state and almost all photoexcited excitons in Si nanocrystals have energies above this value, this process is favorable.

For the larger DPBF concentrations (about 0.8 mM) the increase of PL intensity for the high energy side of the spectral range is caused by DPBF luminescence. At high concentrations it absorbs laser light efficiently and, therefore, luminesces stronger than PSi. In contrast, α-terpinene does not quench PSi PL even at 2 M concentrations. PSi PL quenching means that if the mM concentrations of DPBF are used in photobleaching experiments, energy of almost all excitons is directly transferred to DPBF molecules. This process restricts formation of singlet oxygen and the photobleaching of DPBF mainly takes place via a Type II pathway described above. Thus, the efficiency of photodegradation of organic molecules by singlet oxygen generated by PSi strongly depends on the nature of solvent (due to quenching of singlet oxygen by solvent),

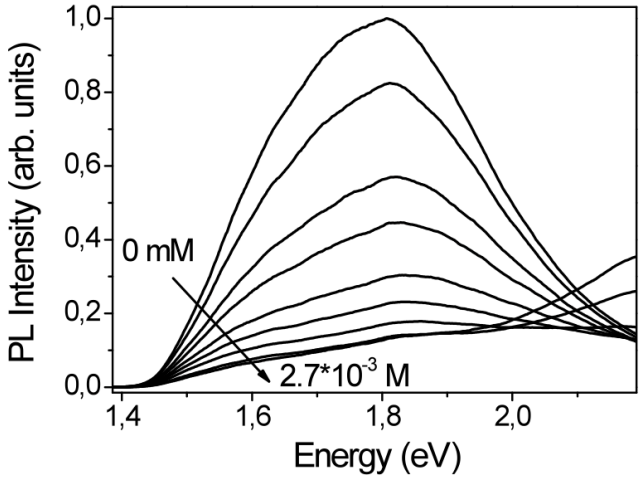

Fig. 19. PL spectra of 0.9 % wt. PSi powder dispersed in DCM containing various concentrations of DPBF, from top to bottom: 0, 35, 70, 100, 210, 350, 700 µM, 1.7, 2.7 mM Note, at high concentrations of DPBF its PL can be clearly seen in the spectral range at higher energies. $E_{ex.}$= 2.54 eV, $I_{ex.}$=500 µW cm^{-2}.

potential quenching of oxygen by the surface of PSi, which will be more pronounced in the case of highly developed surface areas, as well as on the possibility of direct quenching of excitons by direct energy transfer to organic molecules.

Results obtained on efficiency of PSi were used to develop a more general scheme of reaction network with possible quenching routes. This can be used to optimize the efficiency of a sensitizer based on the PSi system.

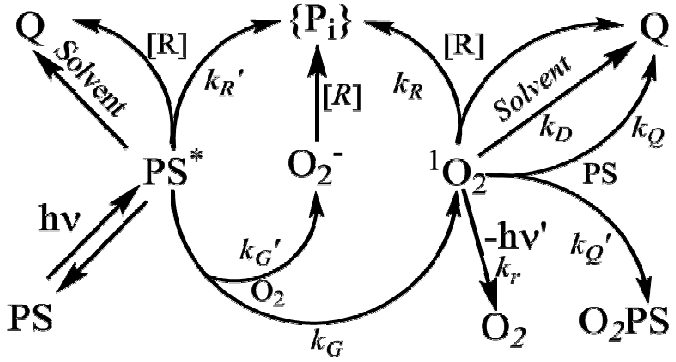

Fig. 20. Sketch of main steps in the process of singlet oxygen quenching in the PSi pore network. Main possible physical and chemical reaction channels in the system: PSi (photosensitizer), light (*hv*), solvent, molecule of reagent (R) and O_2 are indicated.

The general scheme of the mechanisms of quenching of singlet oxygen generated in the pores of in PSi containing organic solvents is sketched in Fig. 20.

We conclude that key singlet oxygen quenching route for PSi is its physical quenching by the PSi pore network due to interaction with high frequency Si-H bonds. Thus the energy of electronic excitation is transferred to vibronic energy of Si-H bonds.

This mechanistic understanding of the phenomena provides the basis for further development of specific reactions of interest for destruction of explosives.

Here we continued the study of degradation of *DPBF* in the presence of singlet oxygen. This compound easily undergoes a 1,4-cycloaddition reaction with singlet oxygen molecules forming an endoperoxide (an overall reaction constant, $Kr = 8 \times 10^8$ L mol^{-1} s^{-1}), which decomposes irreversibly yielding the product 1,2-dibenzoylbenzene. Fig. 21 shows results of the *DPBF* photodegradation experiments performed in the annular recirculating reactor in N_2- and O_2-saturated *F113* containing dispersed *PSi*, under dark conditions and under the 524 nm LED lamp illumination. The concentration of *DPBF* did not change without illumination either in N_2 or O_2 ambience. Also, no photobleaching of *DPBF* was observed under the LED lamp illumination in the absence of *PSi*. A small decrease in the concentration of *DPBF* was found under irradiation of N_2-saturated suspensions of *PSi* by the LED lamp. The same effect was reported earlier, and was explained by direct electronic interaction between triplet excited states of *Si* nanocrystals and *DPBF*. This process is also known as Type I photosensitized oxidation, taking place due to donation and acceptance of protons or electrons, which results in the formation of free-radical ions. An alternative pathway of oxidation is by the photosensitised singlet oxygen (Type II pathway), which can also lead to degradation of organic compounds. Type II process is dependent on the concentration of O_2 molecules in solution. If a solution is O_2-depleted, the shift from Type II to Type I mechanism is favourable. The observed photodegradation of *DPBF* can also be partly related to an incomplete replacement of O_2 by N_2 after bubbling of N_2, or to the presence of physisorbed O_2 on the surface of *PSi*.

When *PSi* was dispersed in an O_2-saturated solution and exposed to the LEDs illumination for several hours, a linear decrease in *DPBF* concentration was observed. This indicates stability of *PSi* photosensitizer during photodegradation of *DPBF*. In contrast to results obtained in our group earlier, here we demonstrated that photodegradation rate of *DPBF* is independent of the O_2 flow rate. The initial rate of *DPBF* photobleaching in the reaction tank was found to be about 5.0×10^{-8} mol L s^{-1}. The reaction rate inside the annular photoreactor recalculated from this number was

found to be $1.3x10^{-6}$ mol L s^{-1}. Despite the more than double the number of the LEDs used (240 versus 96 LEDs), or a five fold increase in the amount of absorbed photons ($4.4x10^{-6}$ Einst s^{-1} *vs.* $8.3x10^{-7}$ Einst s^{-1}) the *DPBF* photodegradation rates in the current study and earlier are nearly equal ($1.3x10^{-6}$ mol L s^{-1} *vs*. $1.2x10^{-6}$ mol L s^{-1}) (see **Fig. 21**,*a*, *b*). This result is explained if the limiting step in the *PSi*-mediated *DPBF* photobleaching is absorption of photons and the formation of excitons in *PSi*, which is coincident with the observed zero-order kinetics of *DPBF* photodegradation.

In order to characterise performance of *DPBF* photobleaching in a particular reactor we earlier used the term "quantum yield of chemical reaction" defined as a ratio of the rate of photobleaching of *DPBF* to the rate of singlet oxygen generation. However, this term corresponds to the utilisation of singlet oxygen in the reaction but not the real efficiency of a photoreactor in the photobleaching process. For this purpose it is better to use the generally accepted overall quantum yield, especially when the mechanism of the photobleaching process is not clear, as in the case of PSi.

Using the number of absorbed photons obtained from the actinometry data and the initial rate of *DPBF* photodegradation the overall quantum yield of *DPBF* photodegradation was found to be $3.0x10^{-3}$, which is five times lower compared to $1.4x10^{-2}$ re-calculated using our earlier data. The obtained data suggest that photobleaching of *DPBF* mediated by *PSi* is not as efficient as it was reported earlier. Moreover, the data leave doubt over the specific mechanisms involved in *PSi*-mediated photodegradation of *DPBF.*

PSi was also tested as singlet oxygen photosensitizer in the oxygenation of α-pinene to pinocarvone in both, batch and flow conditions. However, there was no conversion at all either in the immersed-well quartz reactor with different amounts of *PSi* (0.2 and 0.02 % wt) suspended in CH_2Cl_2 or in CCl_4 after 7 hours of illumination by a 125 W *Hg* lamp, or in the annular recirculating reactor for all the different types of *PSi* used: *PSi*, *PSiI*, and *PSiII* even after 24 hours of illumination by a *Xe* arc or an LED lamp. In the experiments with *PSi* in CCl_4, and also with *PSiI*, and *PSiII* a change of color of *PSi* was observed, which was interpreted as oxidation of the *PSi* powder.

In order to potentially enhance the performance of PSi as a photosensitizer we performed a series of studies on developing a hybrid organic-inorganic sensitizer. A commercially available tetra(4-allyloxy)phenylporphine (TPP) photosensitizer with four terminal double bonds was anchored to PSi surface using photo- and catalytic (Pt) Si-C

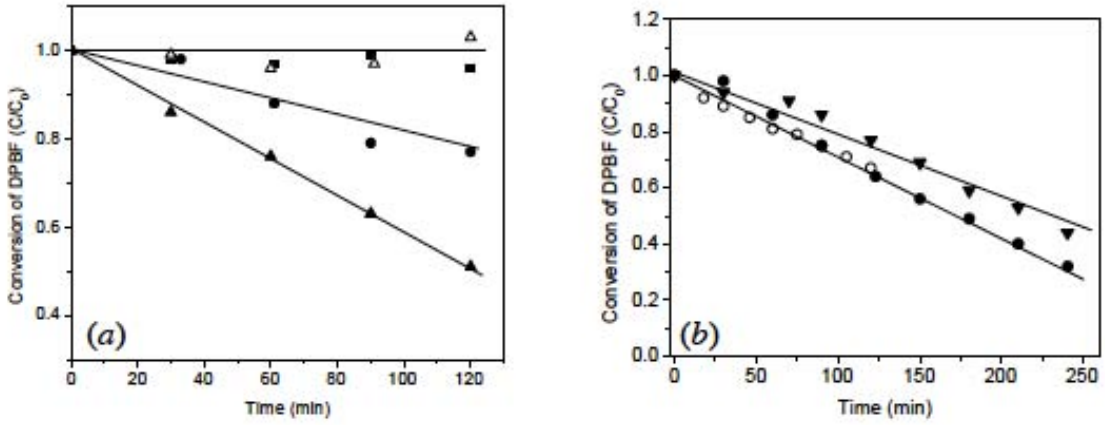

Fig. 21. Photodegradation of 10^{-3} M solution of *DPBF* in *F113* containing 0.2 % wt dispersed *PSi* (250 mL) performed in a recirculating annular reactor and measured by monitoring of the intensity of absorbance at 410 nm in a 1 cm quartz cell. (*a*) N_2 (○, ■) and O_2 (Δ, ▲) saturated solutions under LEDs illumination (Δ, ○) and in dark (▲, ■), N_2 and O_2 flow rates are 30 mL min^{-1}; (*b*) oxygen flow rate influence on oxidation, ○ 30 mL min^{-1}, ● 50 mL min^{-1}, ▼ our earlier data (O_2 flowrate is 50 mL min^{-1}). Reactor temperature is 20 ºC, the liquid flowrate is 40 mL min^{-1}.

bond forming reactions. The prepared TPP-PSi samples were evaluated in the pinene oxygenation reaction in the annular recirculating reactor and a batch tubular reactor with 12 mL volume, both illuminated with 524 nm LEDs. Results are summarized in Table 1. Lower activity of the supported TPP compared to free organic sensitizer was expected. Additional factors affecting activity of TPP are related to the length of the linker between TPP and PSi, which affects the electronic interaction between the two substances and potential quenching of the generated single oxygen by PSi surface, as was noted earlier.

Table 1. Product accumulation rates and reaction rates obtained in the annular recirculating photoreactor and a simple tubular batch photoreactor (*V*=12 mL) in the cases of *TPP* and dye-modified *PSi* prepared *via* thermal, photo, and catalytically activated hydrosilulation, *PSi-S* (*T*), *PSi-S* ($h\nu$), *PSi-S* (H_2PtCl_6) and *PSi-S* ($AlCl_3$), correspondingly.

	TPP	*PSi-S (T)*	*PSi-S (hν)*	*PSi-S (H_2PtCl_6)*	*PSi-S ($AlCl_3$)*
r_0^T, Mol L^{-1} s^{-1}	1.1×10^{-5}	9.6×10^{-8}	1.4×10^{-7}	1.2×10^{-7}	6.8×10^{-7}
r_0^R, mol L^{-1} s^{-1}	1.1×10^{-4}	1.0×10^{-6}	1.5×10^{-6}	1.2×10^{-7}	6.8×10^{-7}
ϕ_R	0.239	0.002	0.003	-	-

5. Development of highly efficient Si-based photochemical flow reactor incorporating porous nanocrystalline silicon and microreactors based on porosified channels of Si wafer.

Scalable photochemical transformation of organic molecules utilizing PSi as an active singlet oxygen generator requires development of prototypes of photochemical reactors. For this purpose we used two reactor configuration options: ordinary flow reactor powered with arrays of green LED's or other light sources (see Fig. 22) and microreactors solely based on micro- and nanostructured bulk (100) Si wafer (see Fig. 23). Different light sources and several flow regimes were used: single-pass, recirculating (semi-batch) and two-phase slug-flow regime (for the microreactor).
The sensitizer efficiency and the reactor throughput and quantum yield were systematically investigated for both systems. Efficiency was defined in terms of productivity (throughput) and quantum yield.

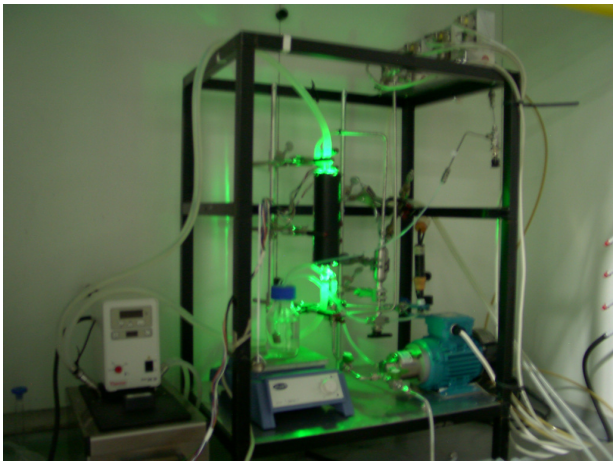

Fig. 22. Photograph of annual recirculating flow reactor powered by green LED arrays (525 nm).

The recirculating annular flow reactor used is a relatively large throughput laboratory system which allows obtaining a reasonable product quantity (5-10 g of isolated product) on a daily basis. The system was equipped with green LEDs and was used both with PSi sensitizer and with organic photosensitizers.
The silicon microreactor chip was produced by wet etching of 3" (100) Si wafers, which results in high-quality vertical wall microchannels. To achieve the desired patterning of channels (Fig. 23a) usually SiN mask was placed on the top of Si wafer. Si etching

process implies the presence of oxidation and reduction reactions in the process. We used hydroxide etching of Si (KOH dissolved in water) which includes a few steps:

1. Oxidation of Si by hydroxyls to form a silicate: $Si+2OH^- +4h^+ = Si(OH)_2^{++}$
2. Reduction of water: $4H_2O = 4OH^- +2H_2+4h^+$
3. Formation of water-soluble complex: $Si(OH)_2^{++}+4\ OH^- = SiO_2(OH)_2^{2-} +2H_2O$

The etching rate of bulk Si for concentrated KOH solution is about 1μm/min.

The channels were 50-350 μm wide and 100-250μm deep (see Fig. 23b). Walls of microreactor have been porosified using stain etching in HF and HNO_3 vapor ambient to achieve a few mictometer thick PSi layer on the top of walls (see Fig. 23c). The reactor was sealed with Pyrex glass plate using anodic bonding (see Fig. 23a). For efficient reaction control the glass-silicon device was placed on a micro-machinned cross-flow heat exchanger. High heat conduction of Si and efficient heat transfer in a micro-heat exchanger ensure that reaction is at constant desired temperature. This is important since light sources are generating excess of heat which must be removed from the system. Such a reactor can be operated in a recirculating mode, to attain maximum conversion, or in a single-pass mode. In the recirculating mode the behavior of the reactor is similar to that of a batch immersed-well photochemical reactor: all reaction volume experience concentration changes from low to high conversion. The only difference is that only a small part of the overall reaction volume is being exposed to light. The efficient illumination of the microreactor results in an overall higher energy-to-product conversion in the microreactor, compared to the immersed-well batch system. In the case of a single-pass the regime of the reactor is different, a steady state is established within the reactor and variation in light intensity, temperature or oxygen concentration could be established along the channel length. This is a more flexible approach. However for complete conversion it requires much longer channels and slower flow rates. The comparison between productivity and quantum yield of oxygenation of annual flow reactor and Si microrectors is demonstrated in Fig. 24.

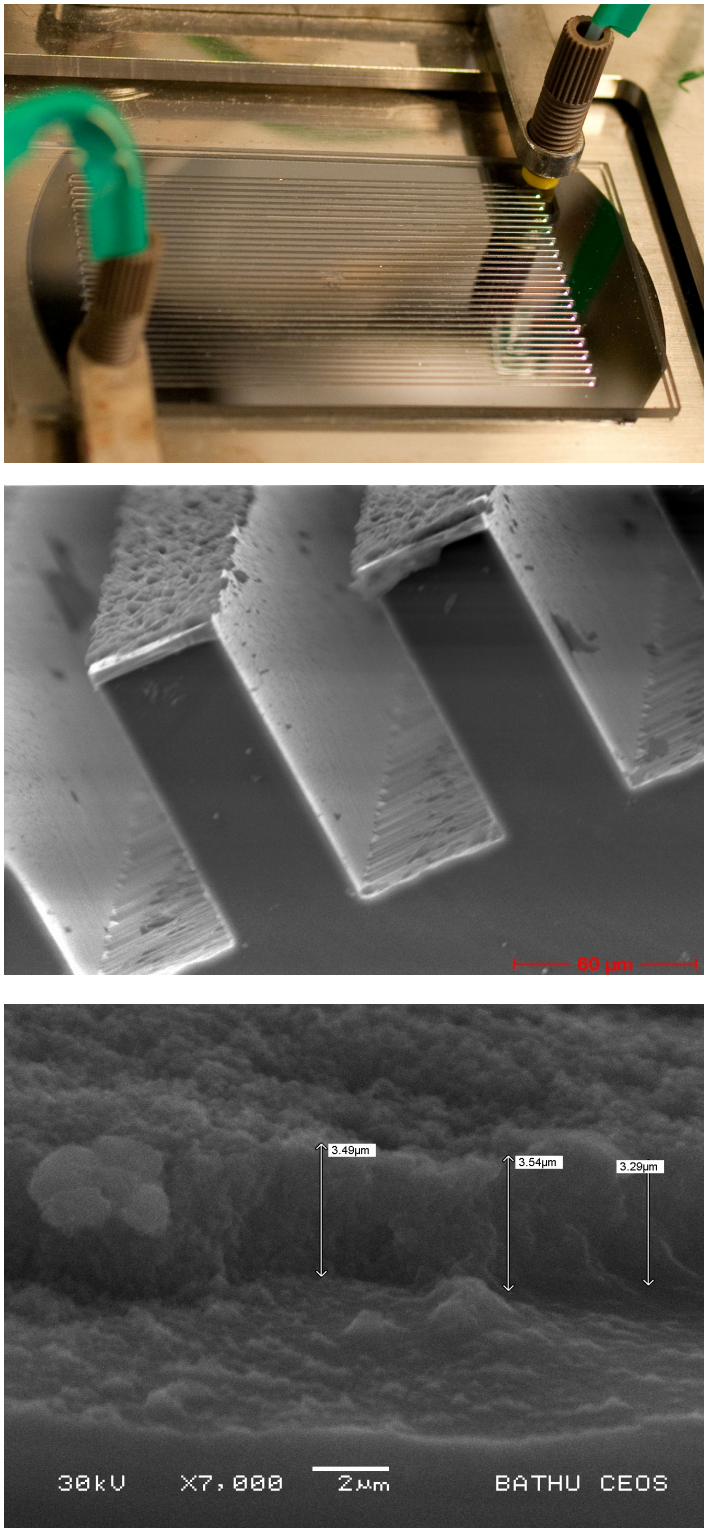

Fig. 23. From top to bottom: photo of bulk Si wafer-based microreactor. SEM image of porosified channels of microreactor. Side view of chemically porosified Si layer covering the channel wall. Length scales are indicated.

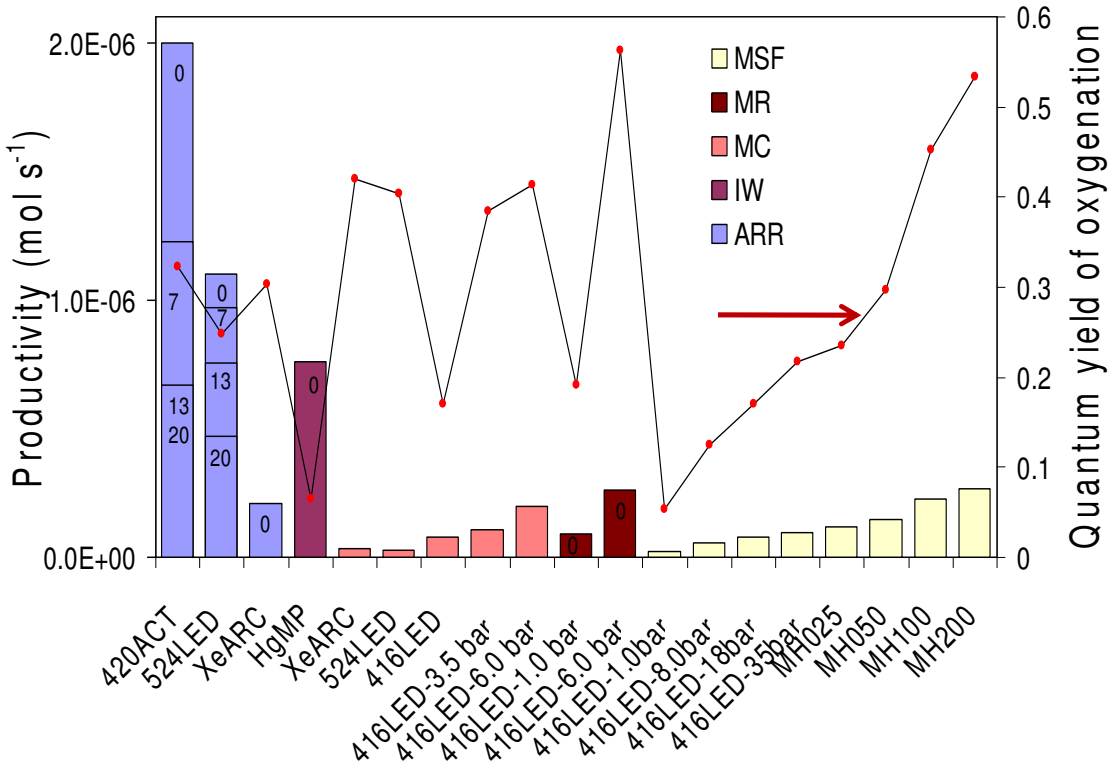

Fig. 24. Productivity and quantum yield of oxygenation of annual flow reactor and Si microrectors. ARR: annular recirculating reactor, MR: microreactor (recirculating mode), MC: microreactor (continuous mode), MSF: microreactor (recirculating two-phase slug flow mode), IW: immersed well reactor.

Experiments have been performed done using pinene singlet oxygen conversion (using organic sensitizers) as a test reaction. Different light sources and pressures indicated along the x-axis have been used.

Figure 24 shows that conventional reactors (ARR) have high productivity, but novel Si wafer-based microreactors have higher quantum yield. Thus, scaling-out microreactors should allow attaining similar productivities at a lower total energy demand.

6. List of publications with acknowledgement of the financial support of U.S. Army (Research Grant No. W911NF0820011d)

1. *Freestanding spherical silicon nanocrystals: A model system for studying confined excitons*
B. Goller, S. Polisski, H. Wiggers, and D. Kovalev
Applied Physics Letters **97**, 041110 s2010d

2. *Efficiency of porous silicon photosensitizer in the singlet oxygen-mediated oxidation of organic compounds*
K. Loponov, B. Goller, A. Moskalenko, D. Kovalev, A. Lapkin
Journal of Photochemistry and Photobiology A: Chemistry **211, 74** (2010)

3. *Silicon nanocrystals dispersed in water: Photosensitizers for molecular oxygen*
B. Goller, S. Polisski, H. Wiggers, and D. Kovalev
Applied Physics Letters **96**, 211901 (2010)

4. *Optimization of a Scalable Photochemical Reactor for Reactions with Singlet Oxygen*
K. Loponov, A. Malkov, M. Barlog, E. Astrova, A. Lapkin
(in preparation for Chem. Eng. J)